Environmental Technology & Innovation 36 (2024) 103803

Contents lists available at ScienceDirect

Environmental Technology & Innovation

journal homepage: www.elsevier.com/locate/eti

Silver recovery from silicon solar cells waste by hydrometallurgical and electrochemical technique

Raffaele Emanuele Russo [a], Muhammad Awais [a], Martina Fattobene [a], Elisa Santoni [a], Rebecca Cavallera [b], Silvia Zamponi [a], Paolo Conti [a], Mario Berrettoni [a,*], Gabriele Giuli [b]

[a] School of Science and Technology, University of Camerino - ChIP Building, Camerino 62032, Italy
[b] School of Science and Technology, University of Camerino - Geology Division, Camerino 62032, Italy

ARTICLE INFO

Keywords:
Silicon solar cells
Experimental design
Electrodeposition-redox replacement
Silver recovery
Waste management
Circular economy

ABSTRACT

In this study, hydrometallurgical and electrochemical methods were combined to achieve an innovative strategy for the effective recovery of the finest silver metal from silicon solar waste. The waste was thoroughly characterized by X-Ray diffraction, Scanning Electron Microscopy, X-Ray Absorption Spectroscopy, and Inductively Coupled Plasma Optical Emission Spectroscopy. A chemometric approach based on experimental design was used to find the best conditions for the leaching process based on a combined base-activated persulfate and ammonia system while a novel method known as electrodeposition-redox replacement was used to recover it. A remarkable pure silver recovery of 98.7±1.4 % was achieved. Additionally, Scanning Electron Microscopy analysis confirmed the enrichment of Ag particles on the electrode. Overall, these promising results showed how flexible the electrodeposition-redox replacement approach is in producing a range of valuable functional materials from intricate hydrometallurgical solutions including multiple metal impurities.

1. Introduction

Silver, being one of the precious metals, holds significance across various aspects of human life due to its distinctive physical and chemical properties (Chernousova and Epple, 2013). In the production of photovoltaic modules, silver is utilized in the metallization process on the front side of silicon solar cells through screen-printing techniques (Cho et al., 2019). While the European Commission did not classify silver as a critical raw material in 2023, its potential criticality should not be overlooked. Silver, positioned on the threshold between non-critical raw materials and the criticality zone, is notable for having a significantly high supply risk score (0.8) (Grohol and Veeh, 2023).

A crystalline silicon solar panel usually consists of an aluminium frame, tempered glass, polymeric sheets of Ethylene Vinyl Acetate (EVA) binding the solar cells together, a junction box, and a polymer back sheet. It also contains valuable elements like silver (Ag) and aluminium (Al) in the form of contacts, silicon (Si) as a wafer, copper (Cu), lead (Pb), and tin (Sn) as constituents of connecting wires (Sah et al., 2022; Chen et al., 2023).

At an industrial level, the recycling of crystalline silicon solar panels primarily emphasizes the retrieval of bulk materials such as

* Corresponding author.
E-mail address: mario.berrettoni@unicam.it (M. Berrettoni).

https://doi.org/10.1016/j.eti.2024.103803
Received 14 May 2024; Received in revised form 15 July 2024; Accepted 17 August 2024
Available online 23 August 2024

glass and aluminium frames. The resulting waste is typically processed at established recycling facilities dedicated to laminated glass and metal (Tao et al., 2020; Sabia et al., 2022). Consequently, valuable materials like silver and copper are often overlooked or disregarded. The significance of recovering silver from spent silicon solar cells cannot be overstated, particularly in light of the increasing demand for silver and the strict environmental regulations in place (Gervais et al., 2023). Moreover, the retrieval of raw materials is crucial for multiple reasons. Conventional metal extraction techniques, such as open-pit mining, can inflict substantial harm on the environment and neighbouring ecosystems. Therefore, employing a metal recovery process based on industrial wastes can mitigate the environmental impact associated with metal production. Additionally, metal recovery generally requires less energy than extracting metals from ore, leading to reduced energy consumption and lower carbon emissions, especially if the recovery rate is comparable to or higher than traditional extraction methods (Russo et al., 2023).

The annual PV market experienced substantial growth, reaching 236 GW worldwide in 2022, marking a 35 % increase compared to the annual capacity in 2021 (Masson et al., 2023). As the production and deployment of photovoltaic systems continue to rise, there is a corresponding increase in end-of-life photovoltaic modules, prompting a growing interest in their recycling. Therefore, disposing of end-of-life solar panels in landfills would be a hazardous approach, displaying a direct threat to the environment (Sah et al., 2022).

From an economic and productivity perspective in the recovery of silver from solar cells, the chemical leaching presents a viable technique. At present, the predominant method for leaching is the utilization of nitric acid, succeeded by precipitation with either NaCl or NaOH or by electrochemical refining. An alternative method involves subjecting the silver to thermal treatments to prepare it before undergoing treatment with nitric acid and subsequently precipitate with NaCl. Additionally, leaching with HCl and the direct precipitation of Ag are also employed as leaching methods (Chen et al., 2024; Zhang et al., 2022; Yue et al., 2022).

This study, in partnership with ORIM s.p.a (a company specializing in metal recovery from solid waste in the Marche, Italy), aims to develop a highly selective process for leaching silver particles and subsequently electrodepositing them through environmentally friendly electrochemical methods. The presence of copper poses a challenge, acting as an antagonist and impeding the achievement of highly pure silver due to the close values of their standard reduction potential (Ag=0.8 V vs SHE and Cu=0.3 V vs SHE) (C.Weast et al., 1984). To address this issue, a combined base-activated persulfate and ammonia system was tested in the leaching process. Persulfate acts as an oxidizing agent and its strong oxidation properties can be activated using a strong base (NaOH). This system is designed to generate a protective hermetic layer of copper (II) oxide, preventing the leaching of copper (Hyk and Kitka, 2017). Design of experiment (DoE) was carried out to find better conditions for silver leaching. In this way the precision is maximized, and specific conclusions can be drawn regarding a hypothesis statement (Leardi, 2009; Bell, 2009). Subsequent to the leaching process, an electrochemical method was employed to recover purest silver metal. Electrochemical recovery of precious/valuable metals includes the deposition of metals onto solid, inert electrodes. In most cases, the concentration of metallic impurities in a solution far exceeds that of the target metals. The prevention of co-deposition of contaminant metals poses a significant challenge when the reduction potentials of these metals are in close proximity. This proximity results a decline in the purity of the recovered product. Thus, the present scenario requires further purification (Shaltry et al., 2017). The electrodeposition-redox replacement (EDRR) approach successfully resolves this issue by applying a pulsed electrodeposition method. This technique, previously reported in the literature, enables the recovery of highly pure silver metal from hydrometallurgical leachate containing copper ions (Elomaa et al., 2018). This procedure allows for the electrodeposit of extremely pure deposits of small quantities of rare metals while keeping their purity intact (Yliniemi et al., 2018). This would be completely consistent with the concepts of sustainable growth and the circular economy (Cui et al., 2023). The key to the method's effectiveness is the spontaneous redox reaction between the less noble and more noble metals. Metallic elements with a lower electrode potential are responsible for the reduction of a dissolved metal (with a higher electrode potential) to zero valence (Yliniemi et al., 2018). Metals dissolved in a solution can be recovered (spontaneously reduced) using this method (Fig. 1). In summary, the aim of this study is to identify the best experimental conditions for the leaching and recovery of silver without impurity.

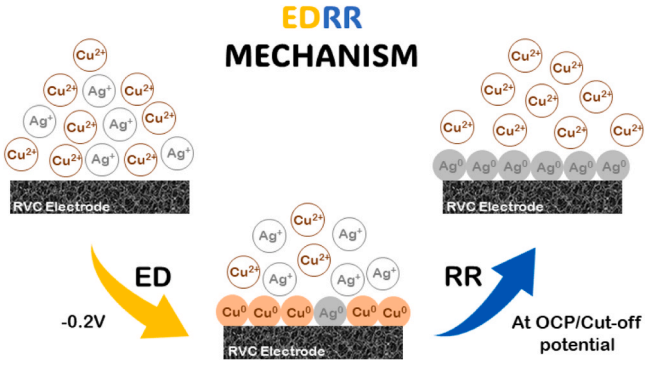

Fig. 1. Mechanism of the electrodeposition-redox replacement.

2. Materials and methods

2.1. Materials and reagents

The silicon solar cells waste used in this study was provided by Orim S.p.a. Reagents and chemicals including nitric acid (65 % pure) and hydrochloric acid (37 % pure) were purchased from Sigma-Aldrich, while ammonia (25 % pure) and Potassium PerSulfate (PPS) from Fluka and sodium hydroxide (pure) from Merck. All reagents and chemicals were used without further modification. Deionized water was employed in the leaching process and for the preparation of solutions for inductively coupled plasma analysis. Multi-element standards (IQC-26) were employed by Agilent.

2.2. Analytical methods

The Inductively Coupled Plasma Optical Emission Spectrometry (ICP-OES) (model Thermo Scientific™ iCAP™ PRO X Duo) was used to measure the metal concentrations. Particle morphology and crystal structure were characterized by Scanning Electron Microscope (SEM-EDX) (model Zeiss Sigma 300) and X-Ray Diffraction (XRD) system (model Philips PW 1830, Cu-kα, graphite monochromator), respectively. Turbomolecular pumped coater (QUORUM Q150T) was used to create a conductive film for SEM-EDX analysis. Copper oxidation state was studied through X-Ray Absorption Spectroscopy (XAS) and spectra were collected in fluorescence mode at the LISA CRG Beamline (BM08) of the European Synchrotron (ESRF) in Grenoble, France (D'Acapito et al., 2019). Electrochemical measurements were carried out by CHI instrument potentiostat (model CHI660A). A HANNA HI 8424 pH-meter was used for pH adjustments. Multivariate analysis was employed with CAT software (Chemometric Agile Tool) (Leardi Riccardo et al., 2024).

2.3. Experimental procedure

The silicon solar cells waste was in the form of dust. We opted to utilize it without undergoing additional processing, thereby avoiding unnecessary increases in time and cost. In order to measure the total amount of the metals (wt% total), aqua-regia was used to dissolve the waste in a duplicate at 350°C, whilst the silver content was measured after the digestion with only HNO_3 (65 %) to avoid its precipitation as AgCl and thus inaccurate analysis. In accordance with the experimental design, two solutions were prepared for the leaching experiments, each with the specified molarity derived from the starting solution (see Table 2). NaOH was added to achieve a theoretical pH of about 13. It is necessary to increase the oxidation properties of persulfate salt. Temperature and stirring rate were kept constant to 25°C and 300 rpm, respectively. Upon completion of the reaction, the solution was filtered and then filled up to the desired volume in a volumetric flask. The metal content (wt% leaching) of the resulting leaching solution was then measured through ICP-OES. The Leaching Efficiency (LE) of each metal was calculated using Eq. 1:

$$LE = \frac{\text{wt\%(leaching)}}{wt\%(total)} \quad x \quad 100 \text{where} wt\% = \frac{[M]x \quad V \quad xDF}{w} \quad x \quad 100 \tag{1}$$

whereas: wt% (leaching) is the metal content leached and wt% (total) is the total metal content in the silicon solar cell waste. M, V, DF, and w are the metal concentrations in leach liquor (mg/L), the volume of leach liquor (L), the dilution factor for the ICP-OES analysis and the weight of sampling (mg), respectively.

Following the leaching process, an electrochemical technique was used to recover silver in a conventional three electrode system including reticulated vitreous carbon (RVC) as the working, a platinum plate as counter, and an Ag/AgCl (3 M KCl) for the reference electrode. The pH was adjusted using a pH meter. Cyclic voltammetry (CV) and electrodeposition-redox replacement (EDRR) techniques were used to efficiently recover metals from the silicon solar cell waste. The determination of metal concentrations was carried out utilizing ICP-OES analysis, while SEM was employed to examine the physical structure of the deposited metal.

2.4. ICP-OES, XAS, XRD, SEM-EDX and EDRR Analysis

The Calibration standards for ICP-OES analysis were assessed by injecting a blank as well as five standard solutions ranging from 1 ppb to 10 ppm. Linear regression of the standard concentrations and the blank-subtracted peak areas of the standards were used to derive a calibration curve. A new calibration curve was measured at the start of each run. ICP-OES operating conditions are listed in Table S1 with more information.

XAS investigation at Cu K-edges (8979 eV) was carried out by means of a Si(111) double-crystal monochromator in 16 bunches mode. Measurements were carried out in fluorescence mode, employing a 12-element solid-state (high purity Germanium) detector (Puri et al., 2019). Spectral profiles were collected using ion chambers filled with argon gas. Pellet was prepared by mixing about 45 mg of cellulose with 45 mg of sample (μTd ≈ 1.5) and by scanning at the Cu K-edge with the following steps: (i) 8828.9–8958.9 eV, step: 5 eV; (ii) 8958.9–9008.9 eV, step: 0.15 eV; (iii) 9008.9–9728.9 keV, k constant step of 0.05 $Å^{-1}$. The energy calibration was performed using a Cu foil, and the same used as standard. The ATHENA software was used for the normalization and XANES analysis (Ravel and Newville, 2005).

For the XRD analysis the Cu X-ray tube was operating at 40 kV and 25 mA. Diffractogram was recorded in the 2-theta range from 5 to 90 with a 0.02 step and 2 s counting time. The sample for X-ray diffraction was prepared as finely ground powder mounted in a brass sample holder by side-loading in order to minimise iso-orientation of the grains.

For SEM-EDX analysis, the sample was pre-treated with the deposition of thin conductive films based on chromium for high-resolution observations. The acquisition parameters are illustrated on the pictures (Fig. 3).

The EDRR process included two sequential stages: step-1, electrodeposition (ED) was performed, where a uniform deposition potential (E_1) was given to the electrode for a preset period (t_1). Subsequently, step-2, known as the redox replacement (RR) process, commenced immediately after the electrodeposition phase. During the RR step, no outside current or potential was applied. Instead, the RR process kept going until either the Open Circuit Potential (OCP) reached a set cut-off potential (E_2) or time (t_2) elapsed, whichever came first. The second step's reaction is quite similar to the conventional cementation reaction in hydrometallurgy (Halli et al., 2017; Eakin et al., 2023). Before conducting the EDRR measurements, Cyclic Voltammetry (CV) experiments were performed on a synthetic solution containing 0.5 mM $Cu(NO_3)_2.2.5\ H_2O$ and 0.5 mM $AgNO_3$ in Britton-Robinson buffer with a pH of 2. The objective was to determine the deposition and stripping properties of the analysed solution, which consists of copper and silver. CV scans ranging from 0.0 V→ −1.0 V→ 1.0 V→0.0 V vs. Ag/AgCl were carried out at a scan rate of 20 mVs^{-1}. Subsequent to the CV analysis, the EDRR parameters in the present study are: E_1 at −0.17 V vs. Ag/AgCl, t_1 was 10 s, and E_2 was cut-off potential which is +0.2 V. During this procedure (Fig. 1), the electrode surface underwent selective enrichment of Ag from a solution that included Cu^{2+} and Ag^{+}. In the ED step, Cu^{2+} underwent reduction and was deposited as elemental copper (Cu) on the electrode. In the RR step that followed, more precious Ag metal ions that were remaining in the solution spontaneously replaced the copper layer that had been formed. The deposited Cu was oxidized by silver ions, resulting in its subsequent dissolution into the solution as Cu^{2+} ions. Concurrently, Ag^{+} ions underwent reduction to metallic silver (Ag), leading to an accumulation of Ag on the electrode. The difference in electrode potentials between Cu/Cu^{2+} and Ag/Ag^{+} causes the spontaneous replacement. Following EDRR measurements, CV and ICP-OES analysis were employed to assess the trace of metals in the solution. Additionally, the metal deposited electrodes were further examined through SEM-EDS analysis.

3. Results and discussion

3.1. Characterization of the spent silicon solar cells

The total metal content in the solar cell waste was determined through ICP-OES (Table 1):

All the other metals are below LOQ of the technique or present in trace amounts, a few mg/kg. Fig. 2 shows the diffractogram of the starting sample, displaying diffraction peaks of silicon with minor peaks due to the presence of metallic silver, copper, iron, tin, and lead. As reported in the figure inset, many metals phases and overlapping peaks making phase identification challenging.

The small broad peak at about 3.44 Å is possible to presence small amount of graphene, whereas the very large band centered at about 26 degree is due to the presence of amorphous phase.

Identifying the metal crystalline phases present within the waste is crucial for planning an effective leaching process and evaluating the leaching solution's ability to dissolve metals. In literature is reported that a silver paste is commonly used for electrical contacts in silicon solar cells. The paste typically comprises three constituents: silver powder, organic vehicle, and glass frit. The shape and size of the silver powder particles, the primary component in this type of conductor, may vary based on the process parameters during its preparation (Tsai and Lin, 2013; Fields et al., 2016). The SEM-EDX analysis in Back-Scattered Electron (BSE) reveals and confirm silver particles with oval shapes and diverse sizes (ranging from 20 to 100 μm) (Fig. 3a shows a typical silver particle). EDX analysis of these particles (Fig. 3b) confirm the presence of metallic silver. Furthermore, examination of the residue post-leaching reveals the presence of relict silver (~10 %, see below) in the form of a dendritic shell rimming an oxide core (Fig. 2c-d). The pre- and post-leaching photos (Fig. 3a–c) highlight how the leaching solution corrodes the silver, dissolving it into the solution.

ICP-OES, XRD and SEM-EDX analyses yielded no information concerning the oxidation state of copper. Thus, XAS analysis played a crucial role in studying the oxidation state of copper, a prerequisite for the application of the leaching process employed. X-ray Absorption Near Edge Structure (XANES) spectra of Cu-solar cell in blue (Fig. S1) displays edge energy peak positions and relative peak intensities compatible with that of metallic copper, thus indicating that copper is mainly in the metallic state and not as oxide.

3.2. Leaching process: mechanism and development

Silver can be oxidized in the presence of a suitable oxidizing agent with a standard electrode potential (E_0) value of 0.8 V vs SHE. In our case we utilized a persulphate activated by a base with a E_0 equal to 2.01 V, which is higher than that of hydrogen peroxide (1.8 V) but lower than ozone (2.1 V) (C.Weast et al., 1984; House, 1961; Furman et al., 2010). Subsequently, in the leaching process, metallic silver undergoes to chemical oxidation, leading to the formation of silver(I) oxide (Eqs.2,3). At this point, Ag_2O readily dissolves in an excess of reagent, forming a cationic silver-ammonia complex (Eq.4). The formation of this complex in solution will enhance the dissolution of Ag from the containing materials. Eq.5 shows the sum of the reaction involved in the leaching process.

$$1^{\circ}\text{reaction} : 2Ag + S_2O_8^{2-} \rightarrow 2SO_4^{2-} + 2Ag^{+} \quad (2)$$

Table 1
ICP-OES analysis of the total amount of metals. The error is relative only to ICP-OES measurements.

Al (wt%)	Ag (wt%)	Cu (wt%)	Fe (wt%)	Sn (wt%)	Pb (wt%)
1.85±0.03	0.65±0.08	0.23±0.07	0.71±0.04	1.10±0.07	0.240±0.008

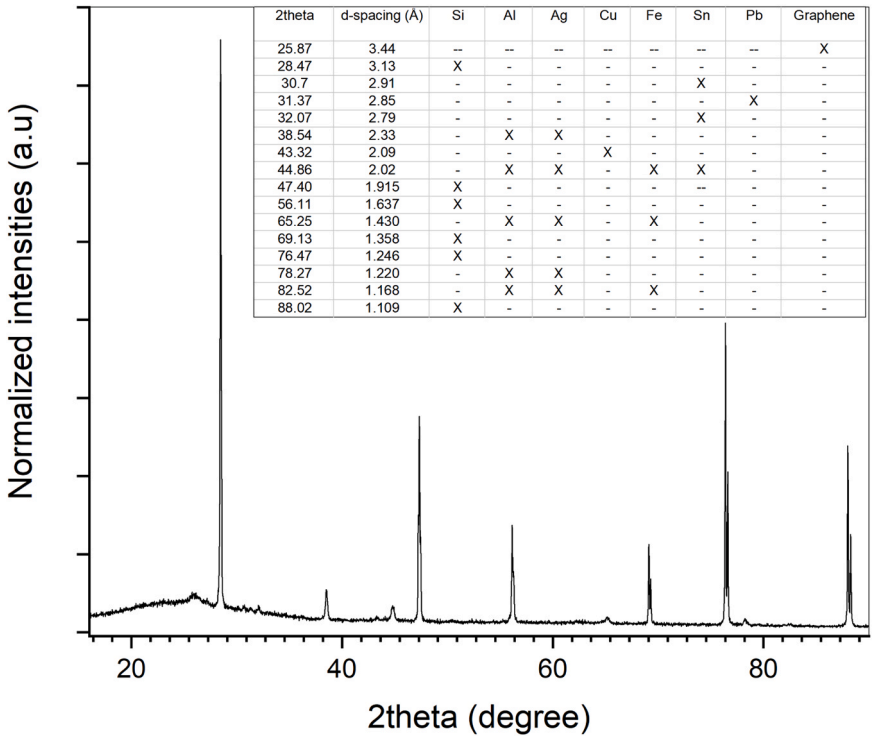

2theta	d-spacing (Å)	Si	Al	Ag	Cu	Fe	Sn	Pb	Graphene
25.87	3.44	--	--	--	--	--	--	--	X
28.47	3.13	X	-	-	-	-	-	-	-
30.7	2.91	-	-	-	-	-	X	-	-
31.37	2.85	-	-	-	-	-	-	X	-
32.07	2.79	-	-	-	-	-	X	-	-
38.54	2.33	-	X	X	-	-	-	-	-
43.32	2.09	-	-	-	X	-	-	-	-
44.86	2.02	-	X	X	-	X	X	-	-
47.40	1.915	X	-	-	-	-	--	-	-
56.11	1.637	X	-	-	-	-	-	-	-
65.25	1.430	-	X	X	-	X	-	-	-
69.13	1.358	X	-	-	-	-	-	-	-
76.47	1.246	X	-	-	-	-	-	-	-
78.27	1.220	-	X	X	-	-	-	-	-
82.52	1.168	-	X	X	-	X	-	-	-
88.02	1.109	X	-	-	-	-	-	-	-

Fig. 2. XRD patterns of silicon solar cells waste.

$$2°\text{reaction} : 2Ag^{+} + 2OH^{-} \rightarrow Ag_2O * H_2O \tag{3}$$

$$3°\text{reaction} : Ag_2O * H_2O + 4NH_3 \rightarrow \quad 2[Ag(NH_3)_2]^{+} + 2OH^{-} \tag{4}$$

$$Sum : \ 2Ag^{+} + S_2O_8^{2-} + 4NH_3 \rightarrow 2[Ag(NH_3)_2]^{+} + \quad 2SO_4^{2-} \tag{5}$$

Regarding copper, which has a lower potential than silver (0.3 V), (C.Weast et al., 1984) it undergoes oxidation by the persulfate present in the solution, leading to the formation of a copper(II) oxide layer that prevents leaching, aided by the strong alkaline solution (Hyk and Kitka, 2017). Copper and silver do not precipitate in a high basic environment due to the formation of soluble complexes with ammonia. The leaching experiments aimed to find the best conditions of the industrial hydrometallurgical process were conducted using a chemometric approach. An experimental design based on 2 (Sah et al., 2022) full factorial design (FFD) was utilized (Table S2) (Jiju, 2023). We examined four independent variables (factors) with the aim of distinguishing the significant ones from those with a negligible effect. The factors considered in modelling and designing the leaching process include the solid/liquid ratio (S/L) of the waste in g/L, the concentration of PPS in mol/L, the reaction time (t_r) of the leaching process expressed in minutes (min) and the concentration of ammonia expressed in molarity (mol/L). The actual values of the factors have been coded to dimensionless levels, as outlined in Table 2. Table 2 also shows the experimental domain of interest (-1 to +1). The experimental domain was carefully chosen, considering both prior experience and relevant literature.

Repeated tests (in bold text in table S2) were carried out between one experimental design and another, and between two experimental groups of the same design to estimate the variance of the experimental error. Moreover, the experimental sequence of the experimental design was randomized to minimize the effects of the uncontrolled factors. The mathematical model to this design is the following (Eq.5):

$$Y = \beta_0 + \sum_{i=1}^{k} . \beta_1 x_1 + \sum_{.} . \sum_{i<j}^{k} . \beta_{ij} x_i x_j \tag{5}$$

where, Y is the response of interest (leaching efficiency of Ag), β_0 a constant, β_i the main effect of the factor i and β_{ij} the interaction coefficients between the i and j factors; the different coefficients will be estimated by multi-linear regression from the results of the experimental design. We considered that three-(or more) factor interactions are neither likely nor important, so it was able to determine the main effects with more degree of freedom.

The factorial design, experimental conditions and responses are given in Table S2. Each line corresponds to an experiment. The expected response is the silver and copper leaching efficiency of the base-activated persulfate and ammonia system. These responses have made it possible to orient our experiments to obtain a leachate with high concentration of silver and low concentration of copper.

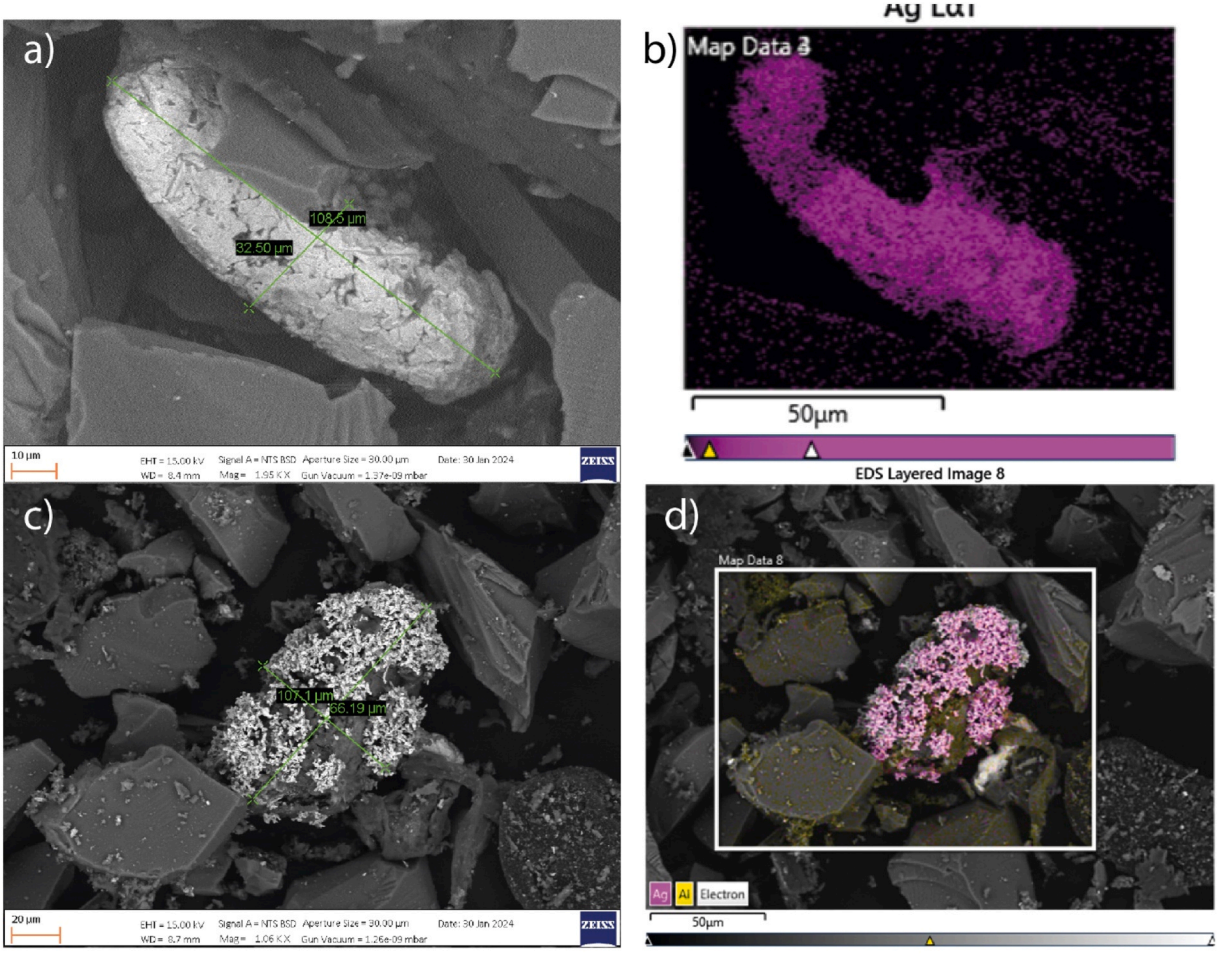

Fig. 3. SEM-EDX analysis: a,b) silver particle in silicon solar cell waste before leaching; c,d) silver particle in silicon solar cell waste after leaching.

Table 2
Independent variables and their coded and actual values used for experimental design of the leaching process.

Factors	Coded variables	Actual values and coded levels		
		-1	0	+1
NH_3 (mol/L)	X_1	0.5	0.9	1.2
Sample (g/L)	X_2	50	75	100
PPS (mol/L)	X_3	0.04	0.10	0.2
Time (min)	X_4	30	45	60

Table S2 also show the experimental point in which the model was validated (coded point 0 of the experimental domain).

Before conducting the analysis of the DoE, silver and copper efficiency was plotted (Fig. 4 and S2). The scatter plots indicate that the silver efficiency of experiments yielding the highest leaching is not correlated with the copper response, as evidenced by the low efficiencies of the latter. However, at low leaching of both metals, a correlation becomes apparent. Furthermore, the scatter plots, which highlight points based on the concentration of each response, reveal this trend where low copper leaching efficiency corresponds to high silver leaching yields (e.g. point 7,15,14 experimental point).

Based on experimental design matrix and observed response (see Table S2) the polynomial model with coded variables was constructed by multiple linear regression. The model presents a R^2_{adj} equal to 98.1 % and a R^2_{pred} about 95.0 %. Analysis of variance (ANOVA) was used to interpret the correlation between the factors and the responses, and to estimate the statistical parameters. The F-values were utilized to assess the statistical significance of the regression equation, while p-values were employed to determine the significance of individual coefficients. Generally, lower p-values indicate a greater significance of the corresponding variables (Johnston, 2014). The model term effects for X_2, X_3, X_4, X_2X_3 and X_3X_4 were deemed significant and had an impact on silver leaching. In contrast, the others model terms were not considered significant, as its p-value exceeded to 0.05. In Fig. 4 is shown the coefficients

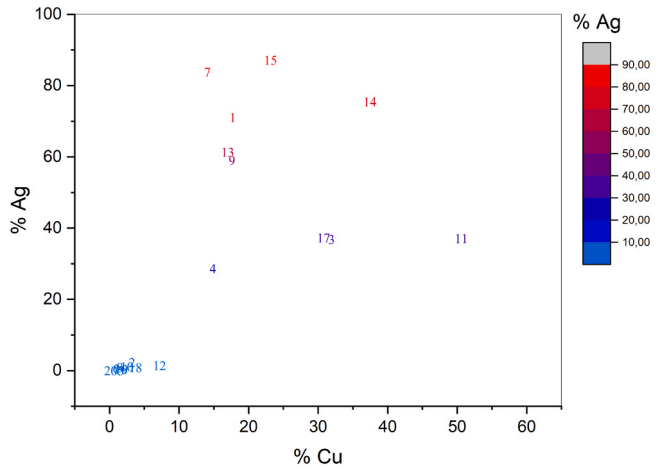

Fig. 4. Scatter plot %Cu versus %Ag (number points correspond to run order). %Ag color map.

plot, providing a clear explanation of the points mentioned above.

Thus, in this model the S/L ratio of the sample and the concentration of PPS have strong significance in the model and so in the silver leaching. As evident from the negative and positive signs, respectively, an increase in the weight of the sample per litre of solution results in a decrease in recovery efficiency. Conversely, increasing the concentration of PPS per litre of solution leads to a high increase in leaching efficiency. Hence, it is rational to choose for the low level of the first factor (50 g/L of sample) and the high level of the second factor, which is 0.2 mol/L of PPS. While time exhibits low significance, increasing the reaction time enhances leaching efficiency. Thus, 60 min is chosen as better condition. The molarity of NH_3 is not significant, so the low level can be chosen (0.5 M). As regard NH_3 molarity, the maximum value was determined based on findings from the literature, indicating that concentration exceeding 1.2 M generally leaches more copper (Hyk and Kitka, 2017). The minimum molarity was selected to avoid working with an overly large experimental domain and to ensure an excess of ammonia. Ammonia generates a silver precipitate that is soluble only with a significant excess of ammonia. Thus, it is crucial to work with a significant excess of ammonia to dissolve the silver into solution effectively. It was also calculated the stoichiometric ratio of ammonia and the metals (it was considered only Cu and Ag ammonia complexes). Upon analyzing the DoE, two additional experiments were conducted to validate the best choice (0.5 M). These experiments were conducted with NH_3 molarity of 0.05 (representing the minimum stoichiometric ratio), and 0.1 (twice the minimum

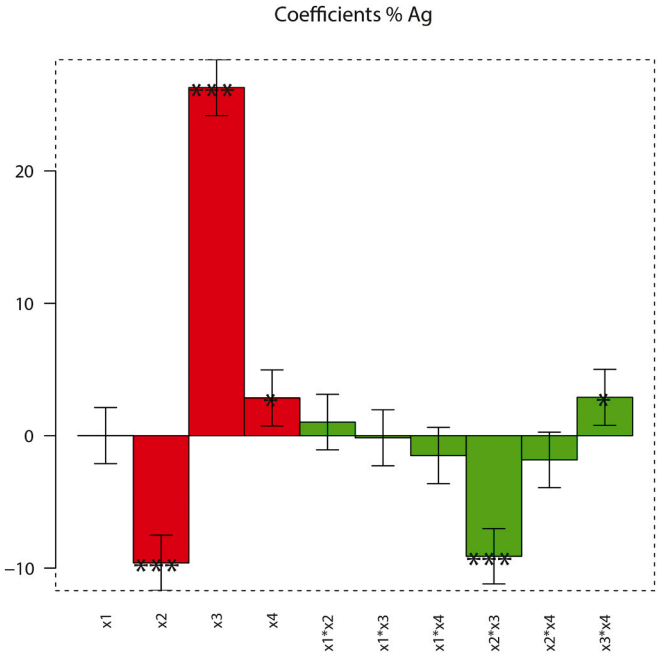

Fig. 5. Coefficients plot of full factorial design. The number of asterisks indicate the significance of coefficients while the green error bars indicate confidential error at 95 % of the coefficients.

stoichiometric ratio) resulting in low silver leaching. Factors such as S/L ratio, PPS concentration, and reaction time were maintained constant at 50 g/L, 0.2 M, and 60 min, respectively, to ensure an ideally occurrence of the reaction with high yields, thereby confirming the suitability of 0.5 M NH_3.

Moreover, there is a notable significance in the interaction between the S/L ratio and mol/L of PPS, while the interaction between mol/L of PPS and time demonstrates lower significance. Thus, the following conditions was chosen as best: 0.5 M of NH_3, 0.2 mol/L of PPS, S/L ratio to 50 g/L and reaction time set to 60 min. Two additional experiments were conducted under these conditions to assess reproducibility. When combined with the two previous tests from the experimental design, an average of 85.0±2.6 % was achieved at a 95 % confidence interval. Additionally, by determining the ratio of extracted silver to leached copper it shows that the silver leaching is 8–10 times higher than that of copper. This outcome aligns well with the utilized leaching process, showcasing successful results. Thus, the low copper content, respect to the silver, was employed as a sacrificial metal for the EDRR process. In conclusion, the model was validated at the central points of the experimental domain, and the experiment was replicated twice. The obtained average was then compared with the predicted value of 27.5±2.4. The validation results showed an average silver leaching efficiency of 29.2±1.0. As evident, the experimental value aligns perfectly with the predicted value.

3.3. Cyclic voltammetry

Prior to conducting EDRR experiments, a cyclic voltammogram was performed using a Glassy Carbon Electrode (GCE). This was done to examine the oxidation and reduction peaks of Ag and Cu, as well as to identify the ideal deposition potential (E_1) and cutoff potential (E_2) for enriching Ag. Fig. 6a illustrates a real solution cyclic voltammogram with a potential range where Ag and Cu oxidation/reduction peaks are predicted. The GCE indicates two reduction peaks in the cathodic scan; the first peak denotes the reduction of Cu^{2+}/Cu at −0.17 V and the second is the reduction of Ag^{+}/Ag at −0.90 V vs. Ag/AgCl, respectively. These peaks can be described as Eqs. 6–7

$$\text{Peak-1: } Cu^{2+} + 2e^{-} \rightarrow Cu^{0} \tag{6}$$

$$\text{Peak-2: } Ag^{+} + e^{-} \rightarrow Ag^{0} \tag{7}$$

The open circuit potential (OCP) or equilibrium potential of the real solution was determined to be +0.2 V vs Ag/AgCl. Consequently, the cutoff potential (E_2) in EDRR was established to be precisely at +0.2 V vs. Ag/AgCl. To verify these peaks' behaviour, a CV analysis of synthetic solution (0.5 mM $Cu(NO_3)_2.2.5\ H_2O$; 0.5 mM $AgNO_3$) was also performed. These results are perfectly aligned with the outcomes obtained from synthetic solution as shown in Fig. S3 and are also in good agreement with the literature (Wang et al., 2024). The parameters obtained from CV analysis were utilized for the enrichment of Ag on RVC electrode in EDRR measurements.

3.4. Recovery of Ag by EDRR

In light of the results obtained from the CV investigations, an EDRR experiment was carried out with copper serving as the sacrificial metal. An illustration of potential with respect to time is presented in Fig. 6b. As evident, during a single EDRR cycle, Copper

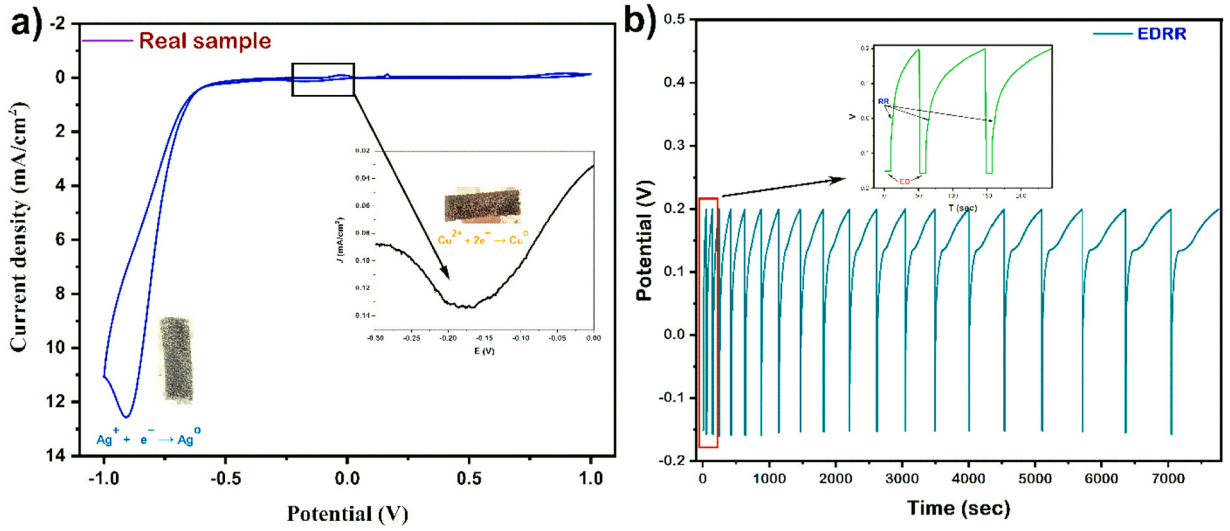

Fig. 6. a) Cyclic voltammetry measurement (0.0 V→ −1.0 V→ 1.0 V→0.0 V vs. Ag/AgCl) of a real solution containing 35 ppm Ag and 11 ppm Cu (Concentration of metals were confirmed through ICP-OES analysis) performed with GCE at a scan rate of 20 mVs^{-1}; b) The potential profile of the RVC electrode during EDRR measurements may be described using the following parameters: $E_1 = -0.17$ V and $E_2 = +0.2$ V vs. Ag/AgCl, $t_1 = 10$ s, and $n = 20$.

(Cu) was first deposited using a short potential pulse at $E_1 = -0.17$ V vs Ag/AgCl for 10 s (t_1). This potential is sufficiently cathodic for Cu to deposit onto the RVC electrode surface long enough for the confirmation of redox replacement (RR) with Ag. The deposition time (t_1) is an adjustable parameter that can be utilized to control the amount of Cu that is deposited onto the RVC electrode during each pulse. In the parameter range examined, it was found that this deposition time (t1 = 10 s) offered the best level for Cu deposition, which was replaced by Ag. Due to a higher concentration of Ag in the solution, Ag was co-deposited onto the electrode surface during the electrodeposition (E1). SEM-EDS analysis revealed that the weight percentage ratio of Cu to Ag (Cu/Ag) on the electrode surface after step 1 was 0.88. Since the redox replacement process can only happen at the deposit/solution interface, it is advantageous to produce a thin layer of imperfect sacrificial metal to get a greater Ag enrichment. Deposition times influence surface purity because, as the deposition time rises (20 s), the thickness of the formed Cu layer grows (Halli et al., 2017). Following the ED step, there was an instantaneous redox replacement (RR) step. During the RR step, the Cu that has been deposited is replaced by Ag^+ ions because of the greater positive potential of the Ag^+/Ag redox pair compared to the Cu^{2+}/Cu redox pair

Moreover, SEM-EDS analysis performed after the EDRR process showed that the electrode had the purest Ag metal deposited on it, with no detectable Cu impurities. Additional details regarding the methodology are elaborated upon in a prior publication (Korolev et al., 2018). It is evident that there is a direct relationship between the number of cycles and the time needed to reach the cut-off potential. This occurs due to the accumulation of Cu on the surface of the electrode, which leads to the process of Ag replacement being more time-consuming. The study proposes that by employing the EDRR approach, it is possible to achieve the highest level of purity for precious metals like Ag, without any concurrent deposition of Cu. According to the literature, (Kowalska et al., 2015) researchers investigated the problems associated with the simultaneous deposition of Cu, which leads to the production of impure products that need additional treatment. A potential advantage of the EDRR method described in this study is that, under optimal deposit duration conditions, precious Ag can predominantly substitute Cu, resulting in the formation of pure surfaces. The EDRR strategy has the advantage of requiring short deposition periods and facilitating the substitution of Ag in open cell systems, depending upon the redox potential difference between the metals. However, as EDRR is performed by cycling between two steps and electrodeposition using only one step with constant parameters, EDRR could be considered as more complicated, expensive, and

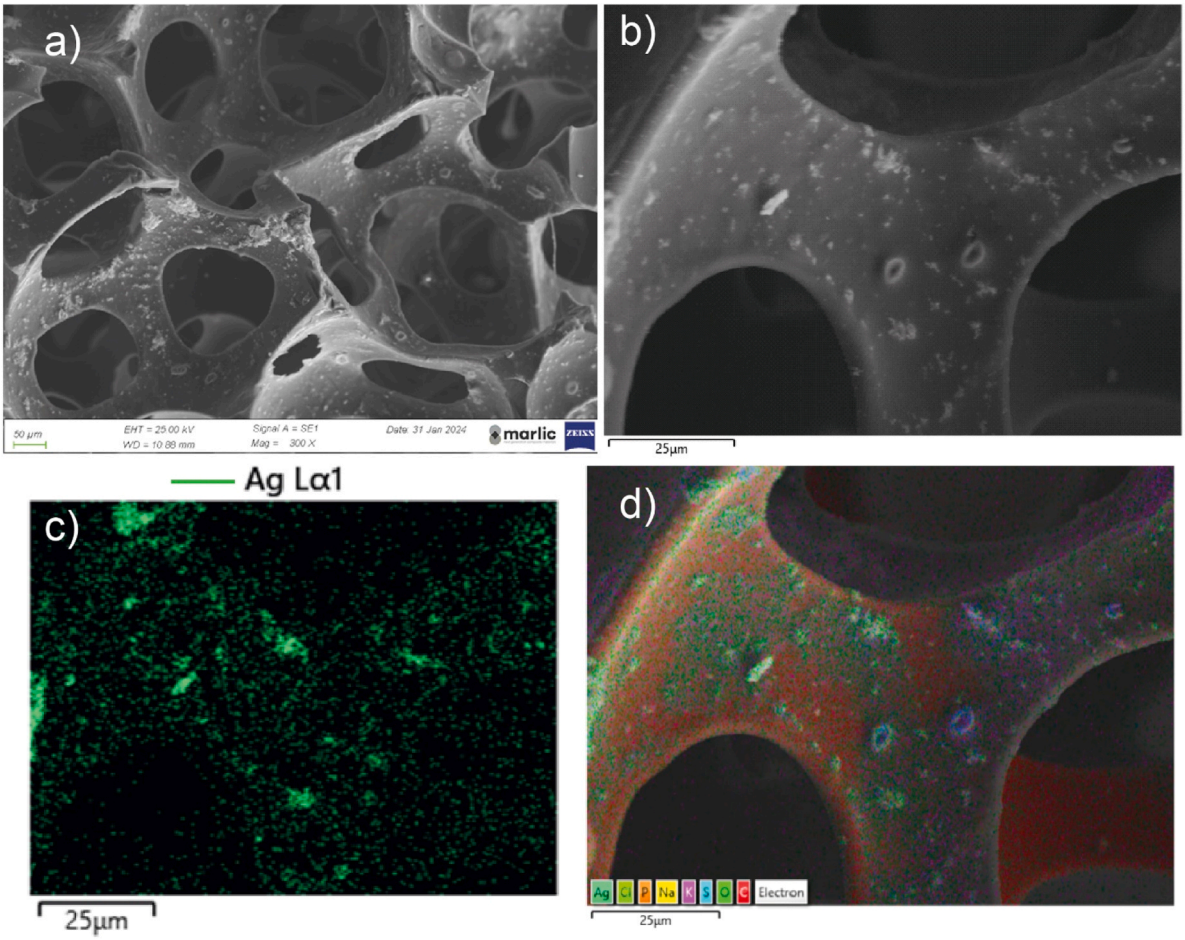

Fig. 7. a,b) SEM images of electrode morphology; c) Ag-deposited EDX map after 20 EDRR cycles using Cu as a sacrificial metal (E1 = −0.2 V vs. Ag/AgCl); d) multi-elemental SEM-EDX map.

time-consuming compared to simple electrodeposition of metals. But EDRR in comparison to direct electrodeposition of Ag, offers high purity with fewer defects. Following the EDRR technique, CV and SWV (square wave voltammetry) analyses were conducted to assess the concentrations of metals in the real solution, as seen in Fig. S4, and Fig. S5, respectively. The EDRR process was carried out four times and ICP-OES analysis was conducted before and after the EDRR process resulting in a recovery yield of 98.7±1.4 %, which is in agreement with the literature (Jung et al., 2016). Also, Elomaa et al (Elomaa et al., 2018). studied the silver recovery from hydrometallurgical bottom ash leachant. The silver was extracted from the leachate as Ag metal with a purity of 99.8 %. The comparison of CV and SWV before and after EDRR treatment provides a clear description of the effectiveness of the EDRR investigation.

3.5. Deposition mechanism and surface morphology

SEM-EDX analysis (Fig. 7a-b) shows the morphology at different magnification levels of the sponge-like structure of the RVC electrode. Fig. 7c shows the spatial distribution of silver $L_{\alpha 1}$ peak while Fig. 5d shows a composite image with a spatial distribution of different elements superposed to the morphology (Elomaa et al., 2018; Ajermoun et al., 2020; Wang et al., 2022; Kanellos et al., 2023). Moreover, Fig. 7c-d revealed that a small number of agglomerates on the electrode surface inside the analysis region were brought on by the presence of potassium and sulphur in the solution, which also deposited alongside silver. The presence of these elements depends on starting materials (PPS). The deposition process based on EDRR yields a more uniform distribution of metals with less agglomeration, in contrast to the cementation method, as reported in the literature (Cui et al., 2023; Hannula et al., 2019). The presence of copper was also checked with SEM-EDX, and no copper particles were found. Moreover, Cu concentration was measured by ICP-OES which confirmed the same values (inside the error) before and after silver deposition.

4. Conclusions

In this study, a simple and efficient process was developed to recover silver from silicon solar cells waste. The leaching process was studied through a design of experiment (DoE) and were found the best conditions. Electrodeposition-redox replacement (EDRR) process was used to recover silver from hydrometallurgical solution originating from silicon solar waste leached by a combined base-activated persulfate and ammonia solution. The main objective of the electrochemical characterization analysis was to achieve silver recovery, effectively mitigate the problem of co-deposition, and provide a feasible strategy for recovering precious metals from hydrometallurgical solutions. The best conditions for silver recovery by EDRR were determined to be $E_1 = -0.17$ V, $E_2 = +0.2$ V vs. Ag/AgCl, and $t_1 = 10$ s, and was recovered by 98.7±1.4 %. Additionally, it is noteworthy to mention that this approach proves to be selective in its recovery of silver and does not require any chemical addition. This unique feature renders this methodology competitive in comparison to conventional processes. Furthermore, SEM-EDX also verified the enrichment of silver on the surface of the reticulated vitreous carbon electrode with no detectable Cu impurities. Overall, EDRR's energy efficiency and feasibility make it an exceptionally competitive approach for silver recovery from side streams of hydrometallurgical processes, with the potential to have a significant influence on the circular economy.

CRediT authorship contribution statement

Mario Berrettoni: Supervision, Project administration, Funding acquisition, Conceptualization. **Gabriele Giuli:** Supervision, Project administration, Funding acquisition, Conceptualization. **Elisa Santoni:** Writing – review & editing, Visualization. **Rebecca Cavallera:** Writing – review & editing, Visualization. **Silvia Zamponi:** Writing – review & editing, Supervision, Resources. **Paolo Conti:** Formal analysis, Data curation. **Raffaele Emanuele Russo:** Writing – original draft, Visualization, Methodology, Investigation, Formal analysis, Data curation, Conceptualization. **Awais Muhammad:** Writing – original draft, Investigation, Data curation. **Martina Fattobene:** Writing – review & editing, Visualization.

Declaration of Competing Interest

The authors declare that they have no known competing financial interests or personal relationships that could have appeared to influence the work reported in this paper.

Data Availability

Data will be made available on request.

Acknowledgements

We acknowledge the Italian CRG beamline at ESRF (LISA-BM08) and we would like to thank D'Acapito Francesco, Alessandro Puri, Jacopo Orsilli and Simone Margheri for assistance in performing the experiment. We also thanks to Engr. Alfredo Mancini, Engr. Roberta Vecchiola and the entire research group of Orim S.p.a. The authors also wish to thank funding by: "Ministero dell'ambiente e della tutela del territorio e del mare – Direzione generale per l'economia circolare" to the project "recupero di materiali critici da rifiuti elettronici" to GG; by FAR UNICAM to the project "REcovery of critical Metals (Pd, Ni, V, Cu, Ag, Sn, Au) from INdustrial wastE (REMINE)" to GG; and funds by MIUR for the PON PhD grant to ER on "recupero dei metalli presenti nei rifiuti dell'industria chimica,

petrolchimica, e farmaceutica" (PI:GG and MB).

Appendix A. Supporting information

Supplementary data associated with this article can be found in the online version at doi:10.1016/j.eti.2024.103803.

References

Ajermoun, N., Lahrich, S., Farahi, A., Bakasse, M., Saqrane, S., El Mhammedi, M.A., 2020. Electrodeposition of silver onto carbon graphite and their catalysis properties toward thiamethoxam reduction: application in food and beverage samples. Heliyon 6 (12). https://doi.org/10.1016/j.heliyon.2020.e05784.

Bell, S., 2009. Experimental design (Published online). Int. Encycl. Hum. Geogr. 672–675. https://doi.org/10.1016/B978-008044910-4.00431-4 (Published online).

C.Weast, R., Astle, J., M, H, Beyer, W., 1984. Handb. Chem. Phys. Vol 64.

Chen, P.H., Chen, W.S., Lee, C.H., Wu, J.Y., 2023. Comprehensive review of crystalline silicon solar panel recycling: from historical context to advanced techniques. Sustainability 16 (1), 60. https://doi.org/10.3390/su16010060.

Chen, P.H., Chen, W.S., Lee, C.H., Wu, J.Y., 2024. Comprehensive review of crystalline silicon solar panel recycling: from historical context to advanced techniques. Sustainability 16 (1). https://doi.org/10.3390/su16010060.

Chernousova, S., Epple, M., 2013. Silver as antibacterial agent: ion, nanoparticle, and metal. Angew. Chem. Int. Ed. 52 (6), 1636–1653. https://doi.org/10.1002/anie.201205923.

Cho, S.Y., Kim, T.Y., Sun, P.P., 2019. Recovery of silver from leachate of silicon solar cells by solvent extraction with TOPO. Sep Purif. Technol. 215, 516–520. https://doi.org/10.1016/j.seppur.2019.01.059.

Cui, L., Yliniemi, K., Vapaavuori, J., Lundström, M., 2023. Recent developments of electrodeposition-redox replacement in metal recovery and functional materials: a review. Chem. Eng. J. 465 https://doi.org/10.1016/j.cej.2023.142737.

D'Acapito, F., Lepore, G.O., Puri, A., et al., 2019. The LISA beamline at ESRF. J. Synchrotron Radiat. 26 (2), 551–558. https://doi.org/10.1107/S160057751801843X.

Eakin, J., Molina, D., Guo, X., Beyenal, H., Ivory, C., 2023. Electrochemical deposition with redox replacement of Lanthanum with Uranium in molten LiCl-KCl. J. Electrochem Soc. 170 (3), 032504 https://doi.org/10.1149/1945-7111/acc09c.

Elomaa, H., Halli, P., Sirviö, T., Yliniemi, K., Lundström, M., 2018. A future application of pulse plating–silver recovery from hydrometallurgical bottom ash leachant. Trans. Inst. Met. Finish. 96 (5), 253–257. https://doi.org/10.1080/00202967.2018.1507320.

Fields, J.D., Ahmad, M.I., Pool, V.L., et al., 2016. The formation mechanism for printed silver-contacts for silicon solar cells. Nat. Commun. 7 https://doi.org/10.1038/ncomms11143.

Furman, O.S., Teel, A.L., Watts, R.J., 2010. Mechanism of base activation of persulfate. Environ. Sci. Technol. 44 (16), 6423–6428. https://doi.org/10.1021/es1013714.

Gervais, E., Kleijn, R., Nold, S., van der Voet, E., 2023. Risk-based due diligence in supply chains: The case of silver for photovoltaics. Resour. Conserv Recycl 198. https://doi.org/10.1016/j.resconrec.2023.107148.

Grohol M., Veeh C. Study on the Critical Raw Materials for the EU 2023.; 2023. doi:10.2873/725585.

Halli, P., Elomaa, H., Wilson, B.P., Yliniemi, K., Lundström, M., 2017. Improved metal circular economy-selective recovery of minor Ag concentrations from Zn process solutions. ACS Sustain. Chem. Eng. 5 (11), 10996–11004. https://doi.org/10.1021/acssuschemeng.7b02904.

Hannula, P.M., Pletincx, S., Janas, D., Yliniemi, K., Hubin, A., Lundström, M., 2019. Controlling the deposition of silver and bimetallic silver/copper particles onto a carbon nanotube film by electrodeposition-redox replacement. Surf. Coat. Technol. 374, 305–316. https://doi.org/10.1016/j.surfcoat.2019.05.085.

House D.A. Kinetics and Mechanism of Oxidations by Peroxydisulfate.; 1961. ⟨https://pubs.acs.org/sharingguidelines⟩.

Hyk, W., Kitka, K., 2017. Highly efficient and selective leaching of silver from electronic scrap in the base-activated persulfate – ammonia system. Waste Manag. 60, 601–608. https://doi.org/10.1016/j.wasman.2016.12.038.

Jiju A. Design of Experiments for Engineers and Scientists. Vol Third Edition.; 2023. doi:doi.org/10.1016/B978-0-443-15173-6.00009-3.

Johnston, R., 2014. Linear Regression Model (Published online). In: Michalos, A.C. (Ed.), Encyclopedia of Quality of Life and Well-Being Research. Springer, *Dordrecht*, pp. 3621–3627. https://doi.org/10.1007/978-94-007-0753-5_1659 (Published online).

Jung, B., Park, J., Seo, D., Park, N., 2016. Sustainable system for raw-metal recovery from crystalline silicon solar panels: from noble-metal extraction to lead removal. ACS Sustain Chem. Eng. 4 (8), 4079–4083. https://doi.org/10.1021/acssuschemeng.6b00894.

Kanellos G., Tremouli A., Tsakiridis P., Remoundaki E. Silver Recovery from Chemical Extract Originating from End-of-life Photovoltaic Panels Using A Microbial Fuel Cell. Published online 2023. doi:10.21203/rs.3.rs-2337564/v1.

Korolev, I., Altınkaya, P., Halli, P., Hannula, P.M., Yliniemi, K., Lundström, M., 2018. Electrochemical recovery of minor concentrations of gold from cyanide-free cupric chloride leaching solutions. J. Clean. Prod. 186, 840–850. https://doi.org/10.1016/j.jclepro.2018.03.177.

Kowalska S., Lukomska A., Los P., Chmielewski T., Wozniak B. Potential-controlled Electrolysis as an Effective Method of Selective Silver Electrowinning from Complex Matrix Leaching Solutions of Copper Concentrate. Vol 10.; 2015. ⟨www.electrochemsci.org⟩.

Leardi, R., 2009. Experimental design in chemistry: a tutorial. Anal. Chim. Acta 652 (1-2), 161–172. https://doi.org/10.1016/j.aca.2009.06.015.

Leardi Riccardo, Melzi C., Polotti G. CAT (Chemometric Agile Tool).2024.

Masson G., De l'Epine M., Kaizuka I. Trends in Photovoltaic Applications 2023 by IEA.; 2023. ⟨www.iea-pvps.org⟩.

Puri, A., Lepore, G.O., D'Acapito, F., 2019. The new beamline LISA at ESRF: performances and perspectives for earth and environmental sciences. Condens Matter 4 (1), 1–7. https://doi.org/10.3390/condmat4010012.

Ravel, B., Newville, M., 2005. Athena, Artemis, Hephaestus: data analysis for X-ray absorption spectroscopy using IFEFFIT. J. Synchrotron Radiat. Vol 12, 537–541. https://doi.org/10.1107/S0909049505012719.

Russo, R.E., Ventura, M., Fattobene, M., et al., 2023. Hydrometallurgical molybdenum recovery from spent catalyst using tartaric acid derived from agrifood waste. ACS Sustain Chem. Eng. 11 (43), 15644–15650. https://doi.org/10.1021/acssuschemeng.3c04318.

Sabia, G., Tammaro, M., Cerchier, P., Salluzzo, A., Brunelli, K., 2022. Treatment and management of the effluents generated by hydrometallurgical processes applied to End-of-Life photovoltaic panels. J. Water Process Eng. 47 https://doi.org/10.1016/j.jwpe.2022.102814.

Sah, D., Chitra, Kumar, S., 2022. Recovery and analysis of valuable materials from a discarded crystalline silicon solar module. Sol. Energy Mater. Sol. Cells 246. https://doi.org/10.1016/j.solmat.2022.111908.

Shaltry, M.R., Yoo, T.S., Fredrickson, G.L., 2017. Experimental Study of Codeposition Electrochemistry Using Mixtures of ScCl3 and YCl3 in LiCl-KCl Eutectic Salt at 500°C. Idaho National Lab doi:10.2172/1392964.

Tao, M., Fthenakis, V., Ebin, B., et al., 2020. Major challenges and opportunities in silicon solar module recycling. Prog. Photovolt. Res. Appl. 28 (10), 1077–1088. https://doi.org/10.1002/pip.3316.

Tsai, J.T., Lin, S.T., 2013. Silver powder effectiveness and mechanism of silver paste on silicon solar cells. J. Alloy. Compd. 548, 105–109. https://doi.org/10.1016/j.jallcom.2012.09.018.

Wang, D., Liang, Y., Zeng, Y., et al., 2024. Highly selective recovery of gold and silver from E-waste via stepwise electrodeposition directly from the pregnant leaching solution enabled by the MoS2 cathode. J. Hazard Mater. 465 https://doi.org/10.1016/j.jhazmat.2024.133430.

Wang, Z., Yliniemi, K., Wilson, B.P., Lundstöm, M., 2022. Targeted surface modification of Cu/Zn/Ag coatings and Ag/Cu particles based on sacrificial element selection by electrodeposition and redox replacement. Surf. Coat. Technol. 441 https://doi.org/10.1016/j.surfcoat.2022.128531.

Yliniemi, K., Wang, Z., Korolev, I., Hannula, P., Halli, P., Lundström, M., 2018. Effect of impurities in precious metal recovery by electrodeposition-redox replacement method from industrial side-streams and process streams. ECS Trans. 85 (4), 59–67. https://doi.org/10.1149/08504.0059ecst.

Yue, Y., Zhuo, Y., Li, Q., Shen, Y., 2022. Experimental and numerical study of extracting silver from end-of-life c-Si photovoltaic solar cells in rotating systems. Resour. Conserv. Recycl. 186 https://doi.org/10.1016/j.resconrec.2022.106548.

Zhang, C., Jiang, J., Ma, E., et al., 2022. Recovery of silver from crystal silicon solar panels in Self-Synthesized choline Chloride-Urea solvents system. Waste Manag. 150, 280–289. https://doi.org/10.1016/j.wasman.2022.07.003.